

# PIB – Printable Intelligent Bot: Learn How to Play Cornhole Game!

University of Bayreuth

Chair of Scientific Computing

Univ.-Prof. Dr. Mario Bebendorf

in cooperation with

isento GmbH & Method Park by UL

By: Antony Youssef

Supervised by : Dr.Jürgen Baier, Thomas Rau, and Sandra Aziz

1st October 2023



# Acknowledgment

It gives me pleasure to thank Dr.Jürgen Baier the CEO of isento GmbH, Thomas Rau a Software Engineer at Method Park by UL, and Sandra Aziz a PhD student at the Chair of Scientific Computing, for their support during this project. In this context, I would like deeply acknowledge Dr.Jürgen Baier for inviting us at isento GmbH and Thomas Rau for inviting us at Method Park by UL. These were great opportunities to visit both companies and performing experimental study as well as practical trials on the robot "pib". Also, I would like to thank Dr.Maximilian Bauer and the Chair of Scientific Computing Univ.-Prof. Dr. Mario Bebendorf for organizing and supervising the modeling seminar.

Finally, I would like to deeply thank Sandra Aziz, for checking and correcting this report.

Thank You !

Bayreuth, October 2023

Antony Youssef

# List of Figures

|      |   |    |
|------|---|----|
| 1.1  | Corn-hole game (Elite Special Events, 2019) . . . . .   | 5  |
| 1.2  | The conditions for hitting the target (T) . . . . .   | 6  |
| 2.1  | Description diagram for a projectile following the simple projectile motion . . . . .   | 7  |
| 2.2  | The experiment for studying the corn bag motion. (a) is the first data set, (b) is the second data set . . . . .  | 8  |
| 2.3  | The analysis of the experimental results for studying the corn bag motion. (a) the analysis for the first data set, (b)the analysis for the second data set . . . . .   | 9  |
| 3.1  | Description for the rotation of links to reach final position . . . . .   | 11 |
| 3.2  | Description for the transformation of point $p$ to reach final position $p'$ . . . . .  | 13 |
| 3.3  | Simple Arm Motion . . . . .   | 15 |
| 3.4  | Description for the launching speed and angle . . . . .   | 16 |
| 3.5  | Description for rotating the basic configuration in clockwise direction by angle by angle $\phi$ . (a) Before the rotation , (b)after the rotation . . . . .  | 17 |
| 3.6  | Description for the arm operation . . . . .   | 18 |
| 3.7  | Description for the arm motion give the upper body motion.(a)Is the basic configuration.(b)after the upper body covered angular displacement $\Psi$ (c) at the launching point, after the arm covered angular displacement of $\Psi + \phi_1$ . . . . . | 19 |
| 3.8  | Description for bag flying diagram . . . . .  | 21 |
| 3.9  | The input for python code to calculate the motion parameters . . . . .  | 22 |
| 3.10 | The motion parameters as output from the Python code . . . . .  | 23 |
| 4.1  | Realistic Simulation for Corn-hole Game using Abaqus . . . . .  | 24 |
| 4.2  | The dimensions of the components of the Corn-hole Game . . . . .  | 25 |
| 4.3  | The input for python code to calculate the motion parameters . . . . .  | 26 |
| 4.4  | The boundary conditions applied on the arm . . . . .  | 26 |
| 4.5  | The boundary conditions applied on the ball . . . . .   | 26 |
| 4.6  | The analysis of the ball's velocity at launching point . . . . .  | 27 |

|   |    |
|---|----|
| 4.7 The motion of the ball during the simulation, the units of velocity is (mm/s).<br>(a)is showing the ball at almost half way, and (b)shows the point when the ball<br>reaches the target . . . . . | 28 |
|---|----|

# Contents

|          |  |           |
|----------|--|-----------|
| <b>1</b> | <b>Introduction</b>  | <b>5</b>  |
| <b>2</b> | <b>Physical Model</b>  | <b>7</b>  |
| 2.1      | Simple Projectile Motion . . . . .                           | 7         |
| 2.2      | Experimental Study on Corn-Bag Motion . . . . .              | 8         |
| <b>3</b> | <b>Simplified Arm Kinematics</b>                             | <b>10</b> |
| 3.1      | Simplified Arm Kinematics . . . . .                          | 10        |
| 3.2      | Simplified Arm Kinematics - With Upper Body Motion . . . . . | 19        |
| 3.3      | Optimization of the Motion Parameters . . . . .              | 20        |
| <b>4</b> | <b>Realistic Simulation for Corn-hole Game using Abaqus</b>  | <b>24</b> |
| 4.1      | Abaqus Model Description . . . . .                           | 24        |
| 4.2      | Abaqus Model Results and Discussion . . . . .                | 27        |
| <b>5</b> | <b>Conclusion and Future Work</b>                            | <b>29</b> |
| <b>6</b> | <b>References</b>  | <b>30</b> |

# Chapter 1

## Introduction

In the past two decades, an increasing interest in robots for games has been boosted. This interest is based on several disciplines such as understanding the human-robot interaction, developing state of art techniques in robotics working mechanisms, and experiencing the advantages of artificial intelligence AI methods as reinforcement learning in developing such robots (Rato et al., 2022).

In this context, the "pib" robot developed by isento GmbH has been invented to be "A Smart Robot For Everyone, Created By All Of Us ". It has been developed so that its parts can be easily printed and its components can be provided by isento in an easy and accessible manner. This work has been developed to help "pib" play the corn-bag hole game as shown in figure 1.1 and in figure 1.2.



Figure 1.1: Corn-hole game (Elite Special Events, 2019)

In this context, the chapters of this report are organized as follows:

Chapter 2: will discuss the flying bag physical model which is based on the simple projectile motion supported by a simple experimental study performed on the corn bag.

Chapter 3: discusses a simple arm motion to achieve the target as shown in figure 1.2 by identifying launch angle  $\phi$  and the velocity  $|\vec{v}|$ .

Chapter 4: is a realistic simulation of the Corn-hole game using Abaqus.

Chapter 5: is a conclusion and suggestions for future work.

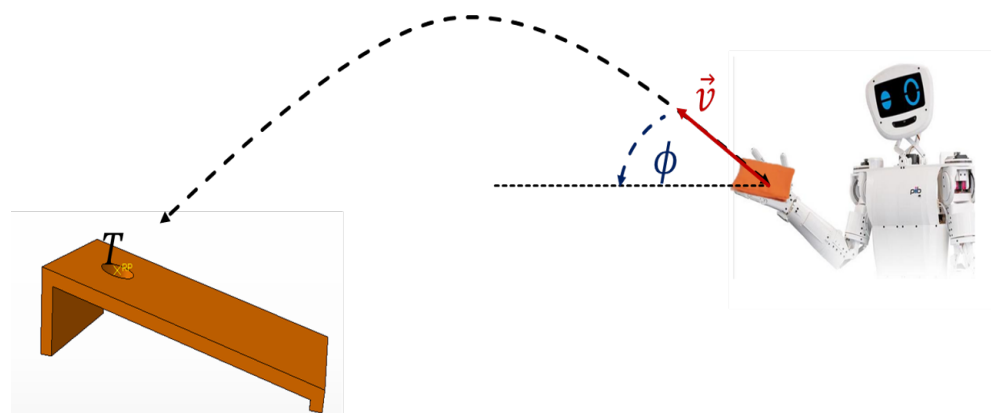


Figure 1.2: The conditions for hitting the target ( $T$ )

Chapter 6: is a list of the references used in this report.

# Chapter 2

## Physical Model

This chapter will discuss the physical model used to describe the motion of a corn bag. In the first section, it is assumed that the motion of a corn bag is following the simple projectile motion. In the second section, an experiment has been conducted, which is used to prove the assumptions provided in the first section.

### 2.1 Simple Projectile Motion

Assuming that the corn bag motion is following the simple projectile motion as explained in Chapter 4 (Serway & Jewett, 2008), indicates that :

1. The only acceleration acting on the projectile is the gravitational acceleration  $g$ , which acts downwards at its center of mass.
2. A projectile act as point mass located at its center of mass
3. A projectile has been launched with velocity  $|v_o|$ , and angle  $\phi$ .
4. All other forces as air resistance are negligible.

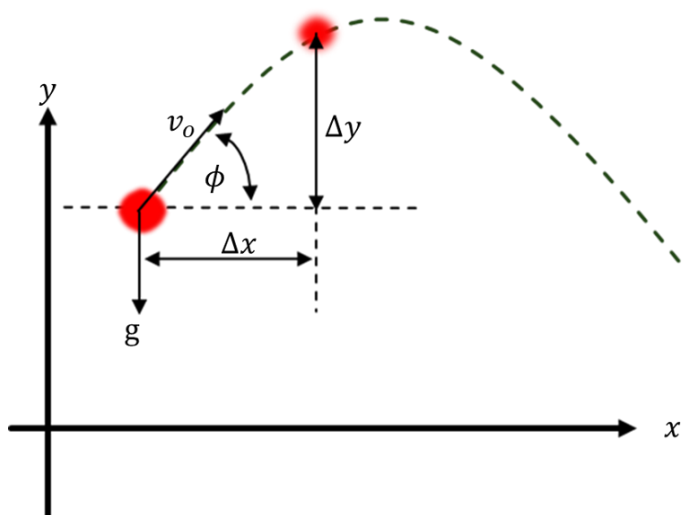


Figure 2.1: Description diagram for a projectile following the simple projectile motion

The mathematical description of the simple projectile motion as shown in figure 2.1, and explained in Chapter 4 (Serway & Jewett, 2008), is :

$$\Delta y = \tan(\phi) \cdot \Delta x - \frac{g}{2 |v_o|^2 \cos^2 \phi} \cdot \Delta x^2 \quad (2.1)$$

## 2.2 Experimental Study on Corn-Bag Motion

Two data sets have been created for studying the projectile motion of the corn bag as shown in figure 2.2. The videos have been captured with a phone camera and have been analyzed using the software "Tracker". A scale of one meter has been identified in the experimental environment to help during the analysis process.

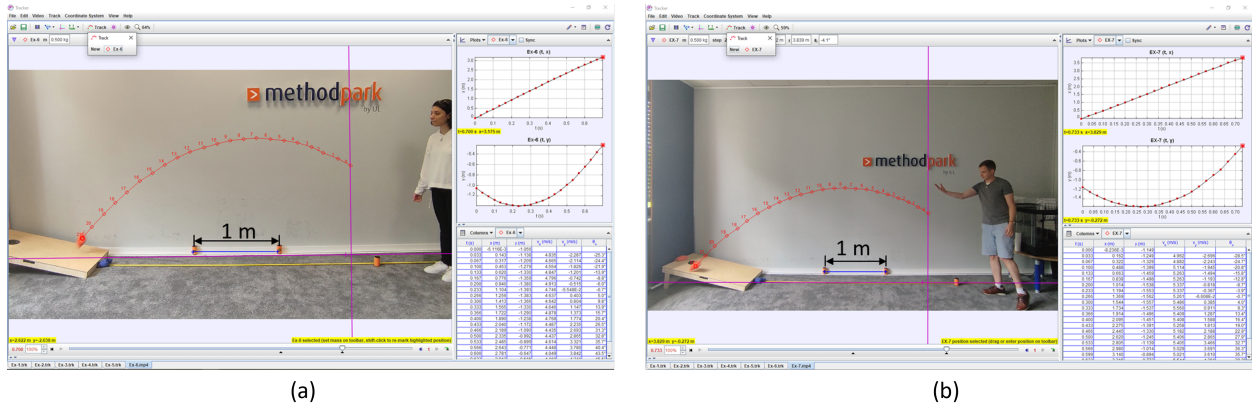


Figure 2.2: The experiment for studying the corn bag motion. (a) is the first data set, (b) is the second data set

These data sets have been analyzed as shown in figure 2.3. The initial velocity  $|v_o|$  and launching angle  $\phi$  have been obtained from the analysis of the experimental data. These values then have been plugged in equation 2.1 and plotted in comparison with the experimental results as shown in figure 2.3. These results show close agreement between the experimental results and the theoretical model. Thus assuming that the corn bag motion will follow the simple projectile motion has been proved to be a valid assumption.

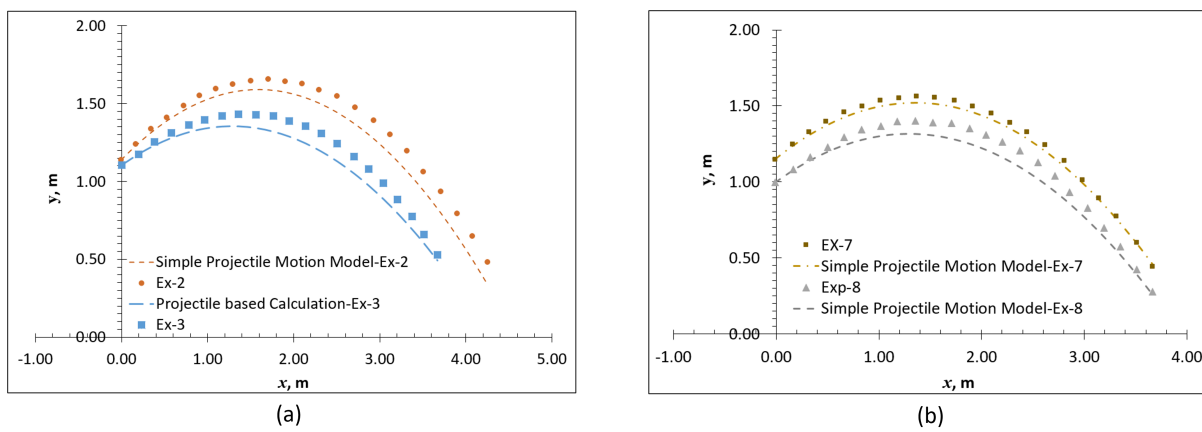


Figure 2.3: The analysis of the experimental results for studying the corn bag motion. (a) the analysis for the first data set, (b)the analysis for the second data set

# Chapter 3

## Simplified Arm Kinematics

In this chapter, the kinematics of a simple arm motion will be presented, followed by a model, taking into account the upper body motion of the robot(chest motion), finally the optimization of the launching speed and angle will be discussed.

The kinematics of the arm will be developed based on the open chain direct kinematics. A manipulator (arm) consists of a series of rigid bodies (links) connected by means of kinematic pairs or joints. The aim of direct kinematics is to compute the pose of the end-effector as a function of the joint variables(angular rotation of joints). That to be done through constructing the transformation matrix (for example : equation 3.7). which will be explained in detail in this section.

On the other hand, the inverse kinematics problem is to determine the joint variables required to achieve the final position and orientation.

In the current model the forward kinematics will be used to construct the relation between the position of the end-effector and the joints variables.

But, the inverse kinematics will not be of relevant use in this model as the relation between joints variables and the end-effector position and orientation will be studied using a different way. This is due to the requirement of the joints variables optimization based on the physical model. As it has been clarified in the previous chapter, for the corn bag to reach the target, the motion parameters should be evaluated, which are the launching velocity  $|v_o|$ , and the angle  $\phi$ . These values are related also to the joints variables. Accordingly, determining the joints variables will be performed through the optimization of the motion parameters as discussed in section 3.3

### 3.1 Simplified Arm Kinematics

Assume having three links ( $L_1, L_2, L_3$ ) connected through three joints(A,B,C), as shown in figure 3.1. So at first the link  $L_1$  is rotated anticlockwise around joint (A) to reach its final position making angle  $\phi_1$  with the basic configuration position, thus reaching configuration "1"

. Then the link  $L_2$  is rotated anticlockwise around joint (B) to reach its final position making angle  $\phi_2$  with the rotated configuration "1", thus reaching configuration "2". Finally, the link  $L_3$  rotated anticlockwise around joint (C) to reach its final position making angle  $\phi_3$  with the rotated configuration "2", thus reaching configuration "3". Thus after these rotations the point  $p$  is transformed to point  $p'$ . Thus correlating the final position to the basic configuration is a must

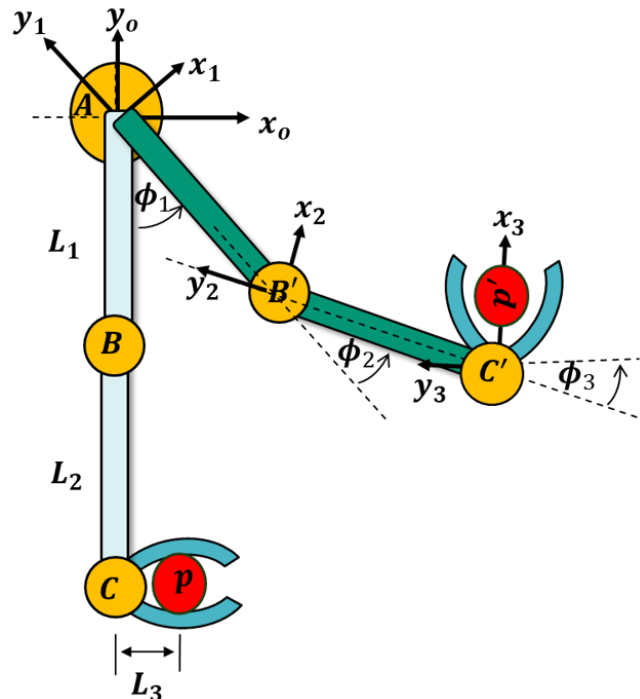


Figure 3.1: Description for the rotation of links to reach final position

to be able to study the relation between them. So the rotation matrix to rotate configuration "1" to "0" is given by equation 3.1 ,while the rotation matrix to rotate configuration "2" to "1" is given by equation 3.2, and finally, the rotation matrix to rotate configuration "3" to "2" is given by equation 3.3, where  $C$  denotes cosine , and  $S$  denotes sine functions for the aforementioned and the upcoming equations.

$$\mathbf{R}_{10} = \begin{bmatrix} C\phi_1 & -S\phi_1 & 0 \\ S\phi_1 & C\phi_1 & 0 \\ 0 & 0 & 1 \end{bmatrix} \quad (3.1)$$

$$\mathbf{R}_{21} = \begin{bmatrix} C\phi_2 & -S\phi_2 & 0 \\ S\phi_2 & C\phi_2 & 0 \\ 0 & 0 & 1 \end{bmatrix} \quad (3.2)$$

$$\mathbf{R}_{32} = \begin{bmatrix} C\phi_3 & -S\phi_3 & 0 \\ S\phi_3 & C\phi_3 & 0 \\ 0 & 0 & 1 \end{bmatrix} \quad (3.3)$$

These rotation matrices are parts of the transformation matrices, as the configuration "1" moved distance  $L_1$  before rotating with angle  $\phi_2$  to construct the configuration "2". Also, the configuration "2" moved distance  $L_2$  before rotating with angle  $\phi_3$  to construct the configuration "3". However, the first configuration did not perform any translational motion with respect to basic configuration. Thus the transformation matrix to transform back configuration "1" to "0" is represented by equation 3.4, while the transformation matrix to transform back configuration "2" to "1" is represented by equation 3.5 , finally the transformation matrix to transform back configuration "3" to "2" is represented by equation 3.6.

$$\mathbf{T}_{10} = \begin{bmatrix} C\phi_1 & -S\phi_1 & 0 & 0 \\ S\phi_1 & C\phi_1 & 0 & 0 \\ 0 & 0 & 1 & 0 \\ 0 & 0 & 0 & 1 \end{bmatrix} \quad (3.4)$$

$$\mathbf{T}_{21} = \begin{bmatrix} C\phi_2 & -S\phi_2 & 0 & 0 \\ S\phi_2 & C\phi_2 & 0 & -L_1 \\ 0 & 0 & 1 & 0 \\ 0 & 0 & 0 & 1 \end{bmatrix} \quad (3.5)$$

$$\mathbf{T}_{32} = \begin{bmatrix} C\phi_3 & -S\phi_3 & 0 & 0 \\ S\phi_3 & C\phi_3 & 0 & -L_2 \\ 0 & 0 & 1 & 0 \\ 0 & 0 & 0 & 1 \end{bmatrix} \quad (3.6)$$

Combining the three transformation matrices into a single one by multiplication will correlate the final configuration with the basic configuration. Thus the total transformation matrix  $\mathbf{T} = \mathbf{T}_{10}\mathbf{T}_{21}\mathbf{T}_{32}$  is given by equation 3.7.

$$\mathbf{T} = \begin{bmatrix} C(\phi_1 + \phi_2 + \phi_3) & -S(\phi_1 + \phi_2 + \phi_3) & 0 & L_1S\phi_1 + L_2S(\phi_1 + \phi_2) \\ S(\phi_1 + \phi_2 + \phi_3) & C(\phi_1 + \phi_2 + \phi_3) & 0 & -L_1C\phi_1 - L_2C(\phi_1 + \phi_2) \\ 0 & 0 & 1 & 0 \\ 0 & 0 & 0 & 1 \end{bmatrix} \quad (3.7)$$

An example to show how the transformation matrix works will be described on point  $p$  transformed to point  $p'$ , as shown in figure 3.2. From this figure the coordinates of the final position of  $p'$  with respect to basic configuration is as described using equation 3.8.

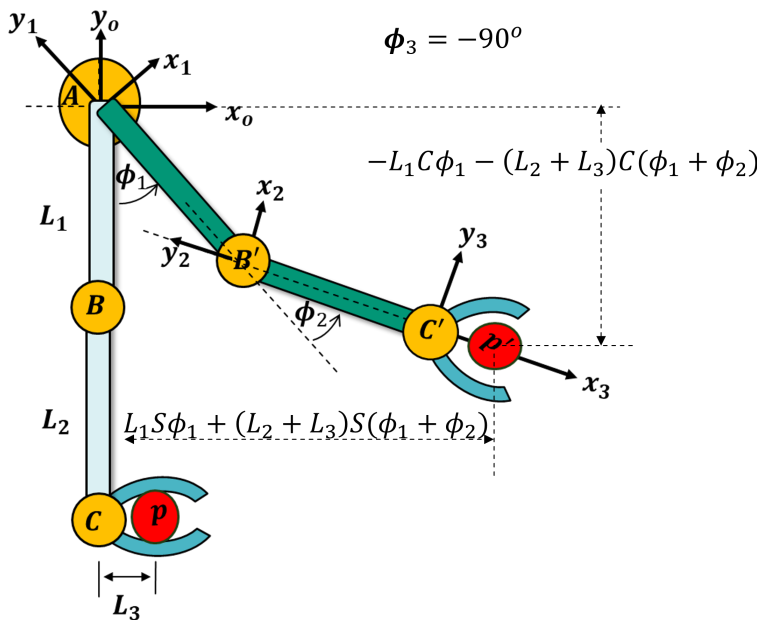


Figure 3.2: Description for the transformation of point  $p$  to reach final position  $p'$

$$\begin{bmatrix} \mathbf{p}' \\ 1 \end{bmatrix}_o = \begin{bmatrix} L_1 S \phi_1 + (L_2 + L_3) S (\phi_1 + \phi_2) \\ -L_1 C \phi_1 - (L_2 + L_3) C (\phi_1 + \phi_2) \\ 0 \\ 1 \end{bmatrix} \quad (3.8)$$

Also, using the transformation matrix the coordinates of the final position of  $p'$  with respect to basic configuration is :

$$\begin{bmatrix} \mathbf{p}' \\ 1 \end{bmatrix}_0 = \mathbf{T} \cdot \begin{bmatrix} L_3 \\ 0 \\ 0 \\ 1 \end{bmatrix}_3 \quad (3.9)$$

The coordinates of  $p'$  with respect to the basic configuration is :

$$\begin{bmatrix} \mathbf{p}' \end{bmatrix} = \begin{bmatrix} L_1 S \phi_1 + L_2 S (\phi_1 + \phi_2) + L_3 C (\phi_1 + \phi_2 + \phi_3) \\ -L_1 C \phi_1 - L_2 C (\phi_1 + \phi_2) + L_3 S (\phi_1 + \phi_2 + \phi_3) \end{bmatrix} = \begin{bmatrix} p'_{xo} \\ p'_{yo} \end{bmatrix} \quad (3.10)$$

It should be mentioned that, the third dimension in equation 3.10 has been dropped as the simple projectile motion is only in 2D. Differentiating equation 3.10 with respect to time will construct the Jacobians for velocity equation :

$$\mathbf{v}_{p'} = \begin{bmatrix} \frac{\partial p'_{xo}}{\partial \phi_1} & \frac{\partial p'_{xo}}{\partial \phi_2} & \frac{\partial p'_{xo}}{\partial \phi_3} \\ \frac{\partial p'_{yo}}{\partial \phi_1} & \frac{\partial p'_{yo}}{\partial \phi_2} & \frac{\partial p'_{yo}}{\partial \phi_3} \end{bmatrix} \cdot \begin{bmatrix} \dot{\phi}_1 \\ \dot{\phi}_2 \\ \dot{\phi}_3 \end{bmatrix} \quad (3.11)$$

This equation can be represented in terms of the specific three velocity Jacobins equation :

$$\mathbf{v}_{p'} = \begin{bmatrix} J_1 & J_2 & J_3 \end{bmatrix} \cdot \begin{bmatrix} \dot{\phi}_1 \\ \dot{\phi}_2 \\ \dot{\phi}_3 \end{bmatrix} \quad (3.12)$$

Where  $J_1$  represents the velocity Jacobins related to the angular velocity  $\dot{\phi}_1$ ,  $J_2$  is representing the velocity Jacobins related to the angular velocity  $\dot{\phi}_2$ , and  $J_3$  represents the velocity Jacobins

related to the angular velocity  $\dot{\phi}_3$ , as described using equations 3.13, 3.14, and 3.15 respectively.

$$J_1 = \begin{bmatrix} L_1 C\phi_1 + L_2 C(\phi_1 + \phi_2) - L_3 S(\phi_1 + \phi_2 + \phi_3) \\ L_1 S\phi_1 + L_2 S(\phi_1 + \phi_2) + L_3 C(\phi_1 + \phi_2 + \phi_3) \end{bmatrix} \quad (3.13)$$

$$J_2 = \begin{bmatrix} L_2 C(\phi_1 + \phi_2) - L_3 S(\phi_1 + \phi_2 + \phi_3) \\ L_2 S(\phi_1 + \phi_2) + L_3 C(\phi_1 + \phi_2 + \phi_3) \end{bmatrix} \quad (3.14)$$

$$J_3 = \begin{bmatrix} -L_3 S(\phi_1 + \phi_2 + \phi_3) \\ L_3 C(\phi_1 + \phi_2 + \phi_3) \end{bmatrix} \quad (3.15)$$

For considering simple arm motion, as shown in figure 3.3, the values for  $\dot{\phi}_2, \phi_2 = 0$  and  $\dot{\phi}_3, \phi_3 = 0$ . Thus the velocity Jacobin will be reduced to only the first Jacobin, so  $\mathbf{v}_{p'} = J_1 \cdot \dot{\phi}_1$

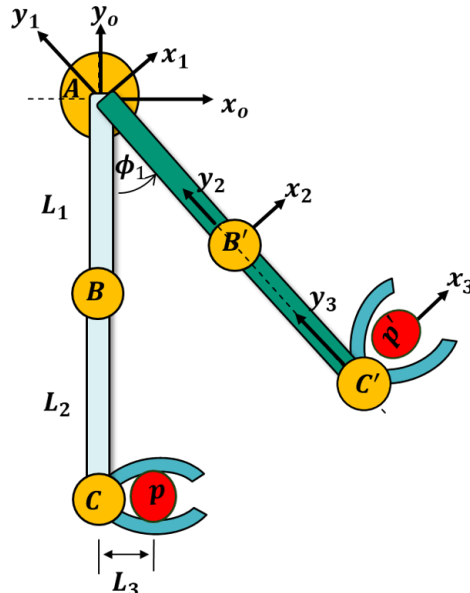


Figure 3.3: Simple Arm Motion

$$J_1 = \begin{bmatrix} \tilde{R} C(\phi_1) - L_3 S(\phi_1) \\ \tilde{R} S(\phi_1) + L_3 C(\phi_1) \end{bmatrix}, \quad \tilde{R} = L_1 + L_2 \quad (3.16)$$

And, the speed can be calculated using the absolute value of the first Jacobin as described using equation 3.17.

$$|v_{p'}| = R \cdot \dot{\phi}_1, R = |J_1| = \sqrt{\tilde{R}^2 + L_3^2} \quad (3.17)$$

The launching angle is calculated based on dividing the two components of the first Jacobin as described using equation 3.18. The diagram for the speed and the launching angle is presented in figure 3.4. The derivation of equation 3.18 is described in equation 3.19 .

$$\frac{J_{12}}{J_{11}} = \frac{\tilde{R} S(\phi_1) + L_3 C(\phi_1)}{\tilde{R} C(\phi_1) - L_3 S(\phi_1)} = \tan(\phi_1 + \phi) \quad (3.18)$$

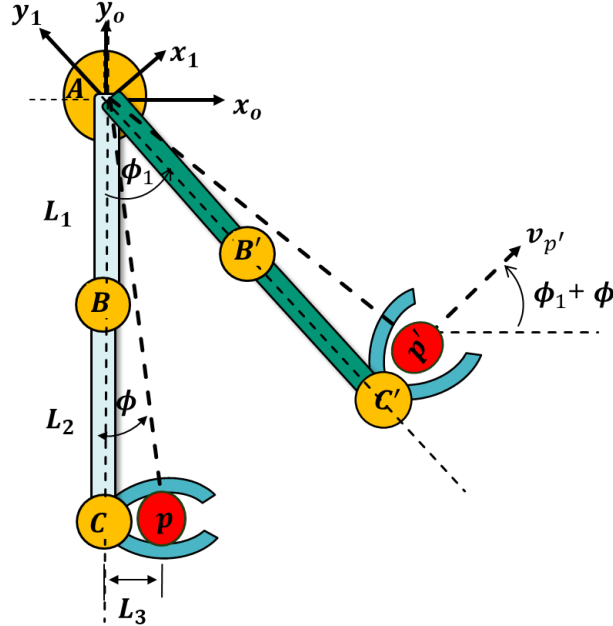


Figure 3.4: Description for the launching speed and angle

$$\frac{J_{12}}{J_{11}} = \frac{\tilde{R} S(\phi_1) + L_3 C(\phi_1)}{\tilde{R} C(\phi_1) - L_3 S(\phi_1)} = \frac{\frac{S(\phi_1)}{C(\phi_1)} + \frac{L_3}{\tilde{R}}}{1 - \frac{L_3}{\tilde{R}} \frac{S(\phi_1)}{C(\phi_1)}} = \frac{\tan(\phi_1) + \tan(\phi)}{1 - \tan(\phi) \tan(\phi_1)} = \tan(\phi_1 + \phi) \quad (3.19)$$

Based on this description, the launching angle is  $\phi_1 + \phi$ , however the arm will move only by an angle  $\phi$ . So it is not recommended to have two angles for this model. As the angle  $\phi$  is difficult to be measured, also it will change with changing the projectile shape and the size of the robot's hand. To solve this issue, the basic configuration will be rotated clockwise by an angle  $\phi$ , thus making the projectile object and the shoulder joint(A) on the same vertical line

as shown in figure 3.5. In practice, it should be ensured, even using visual inspection, that the projectile object and the shoulder are on the same vertical line.

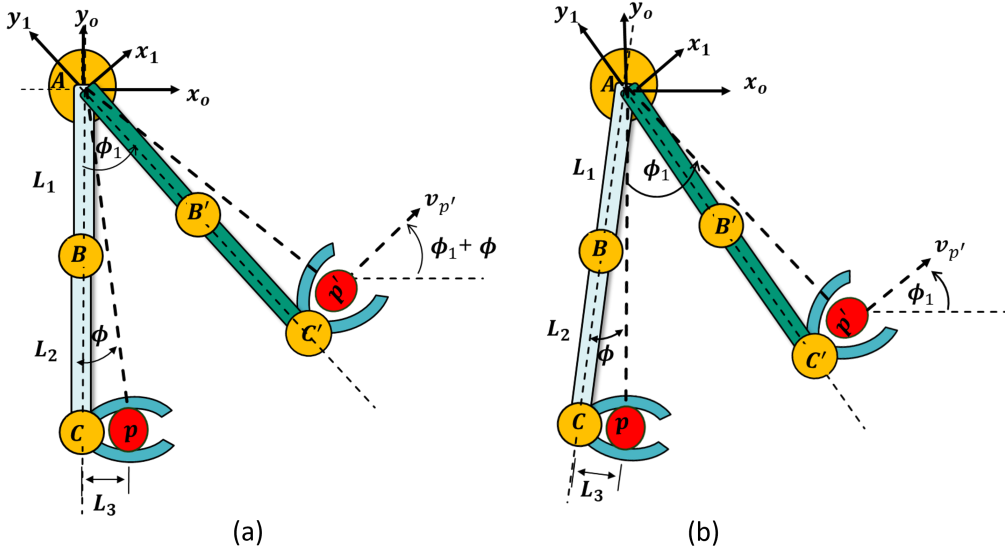


Figure 3.5: Description for rotating the basic configuration in clockwise direction by angle by angle  $\phi$ . (a) Before the rotation , (b)after the rotation

$$J_1 = \begin{bmatrix} \tilde{R} C(\phi_1 - \phi) - L_3 S(\phi_1 - \phi) \\ \tilde{R} S(\phi_1 - \phi) + L_3 C(\phi_1 - \phi) \end{bmatrix} \quad (3.20)$$

Given this modification the first Jacobins equation 3.16 is modified to equation 3.20. The analysis of this Jacobins will show that the speed is the same as equation 3.17 , and the launching angle is  $\phi_1$ .So, given this modification, at the launching instance, the angular displacement is the same as the launching angle.

The correlations between the launching angle  $\phi_1$  , angular velocity  $\dot{\phi}_1$  ,and angular acceleration  $\ddot{\phi}_1$  are provided using newton equations for rotational motion described by equations 3.21, 3.22, and 3.23.

$$\phi_f = \phi_o + \ddot{\phi}t \quad (3.21)$$

$$\phi_f - \phi_o = \dot{\phi}_o t + \frac{1}{2} \ddot{\phi} t^2 \quad (3.22)$$

$$\dot{\phi}_f^2 = \dot{\phi}_o^2 + 2\ddot{\phi}(\phi_f - \phi_o) \quad (3.23)$$

Then,  $\dot{\phi}_1$  could be evaluated using equation 3.17, assuming that the launching speed and the launching angle are known. These parameters will be evaluated in the last section "Optimization of the Motion Parameters". Thus, the  $\dot{\phi}_1$  is equal to :

$$\dot{\phi}_1 = \dot{\phi}_f = \frac{|\mathbf{v}_{p'}|}{R} \quad (3.24)$$

where,  $\dot{\phi}_f$  is the final angular velocity before the projectile starts flying. The angular acceleration is :

$$\ddot{\phi} = \frac{\left(\frac{|\mathbf{v}_{p'}|}{R}\right)^2}{2 \cdot \phi_1} \quad (3.25)$$

And the time required using this angular velocity to reach the target angular speed equation 3.24 is :

$$t = \frac{2 \cdot \phi_1}{\frac{|\mathbf{v}_{p'}|}{R}} \quad (3.26)$$

These values could be presented on a diagram as shown in figure 3.6. Thus, at the braking point the arm angular velocity  $\dot{\phi}_1$  should be  $\dot{\phi}_f$  to achieve the designed launching speed  $|\mathbf{v}_{p'}|$ , and at the same time the launching angle  $\phi_1$

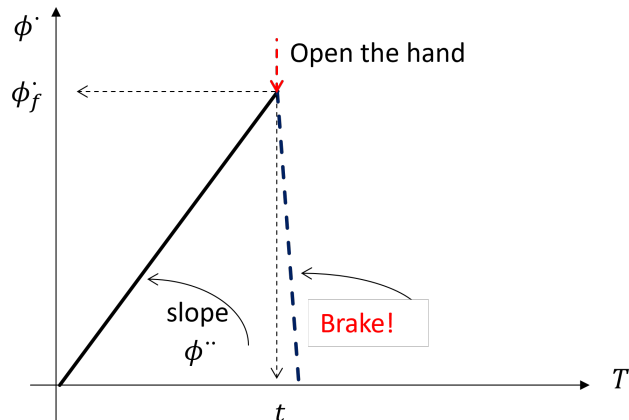


Figure 3.6: Description for the arm operation

The model developed in the previous section could be easily extended to include the upper body motion. As shown in figure 3.7 the upper body will rotate by angle  $\Psi$ , then the arm will rotate by angle  $\Psi + \phi_1$ . The arm and upper body could rotate simultaneously, however for this model, the upper body should finish its motion and stop before the arm starts its motion. In other words, the upper body should reach its final destination covering angle  $\Psi$ , before the arm starts its motion to launch the corn bag, so the angular displacement by upper body is constant by angle  $\Psi$  at the launching time. For the simultaneous motion to be considered which will be based on developing relative velocity between the arm and the upper body, similar mathematical derivation to the previous section is required, but in the current model only the simple model will be illustrated. The simultaneous model could be developed in the future work.

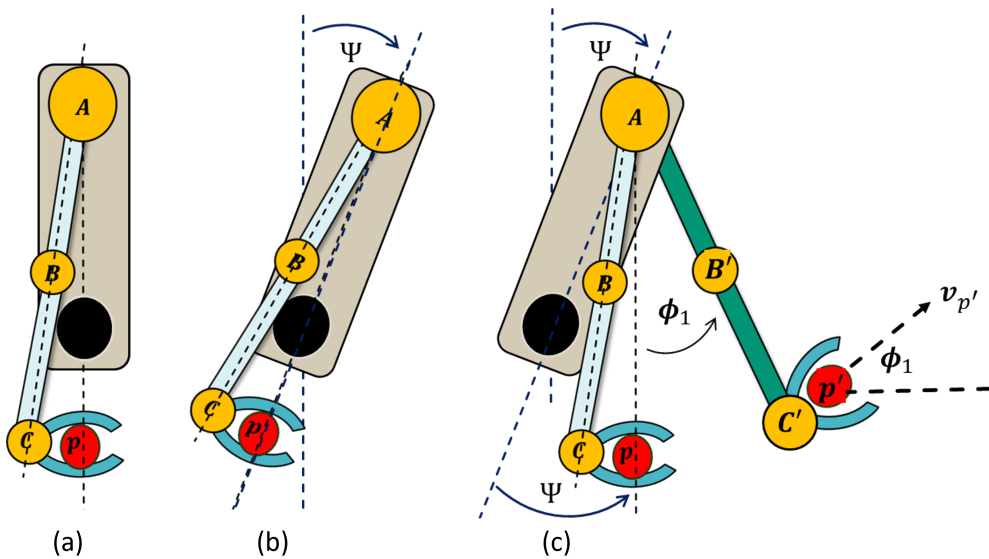


Figure 3.7: Description for the arm motion given the upper body motion.(a)Is the basic configuration.(b)after the upper body covered angular displacement  $\Psi$  (c) at the launching point, after the arm covered angular displacement of  $\Psi + \phi_1$

The calculated values for the rotation of the arm given by equations 3.25 and 3.26, should be updated to take into account the rotation of angle  $\Psi$ . Assuming the values for  $|v_{p'}|$  and  $\phi_1$  are

know, the angular acceleration is :

$$\ddot{\phi} = \frac{\left(\frac{|\mathbf{v}_{p'}|}{R}\right)^2}{2 \cdot (\Psi + \phi_1)} \quad (3.27)$$

And the time required using this angular velocity to reach the target angular speed equation 3.24 is given by :

$$t = \frac{2 \cdot (\Psi + \phi_1)}{\frac{|\mathbf{v}_{p'}|}{R}} \quad (3.28)$$

Thus, at the braking point figure 3.7(c) the arm's angular velocity  $\dot{\phi}_1$  should be  $\dot{\phi}_f$  to achieve the designed launching speed  $|\mathbf{v}_{p'}|$ , and at the same time the launching angle  $\phi_1$ . From equation 3.27 and 3.25, the value for the the angular acceleration is reduced in the current model assuming that  $|\mathbf{v}_{p'}|$  and  $\phi_1$  are equal in both cases. However, this angle  $\Psi$  should be optimized based on the mechanical system of the upper body. The analysis for combined optimization of  $\Psi + \phi_1$ , will not be discussed in this work, only the optimization of  $|\mathbf{v}_{p'}|$  and  $\phi_1$  will be investigated in next section.

### 3.3 Optimization of the Motion Parameters

Assume that the design values for  $|\mathbf{v}_{p'}|$  and  $\phi_1$  are required for the bag to be launched so as to hit the target as shown in figure 3.8. Thus, one possibility could be assuming the angle and solving for the launching velocity using equation 2.1. Rearranging this equation will lead to :

$$|\mathbf{v}_{p'}|^2 = \frac{g \cdot \Delta x}{S(2\phi_1) - 2 \cdot C^2(\phi_1) \cdot \frac{\Delta y}{\Delta x}} \quad (3.29)$$

Thus, for every launching angle, there will be launching velocity to reach the target. However, optimizing the launching velocity to minimum value is recommended as it will reduce the required torque to induce the motion. The torque for a rotating arm is equal  $I \cdot \ddot{\phi}$  (Torque and Rotational Motion Tutorial, n.d.), where  $I$  is the moment of inertia of the arm. The angular acceleration and the launching velocity are directly proportional as described in equation 3.25,

so optimizing the launching velocity will reduce the required torque.

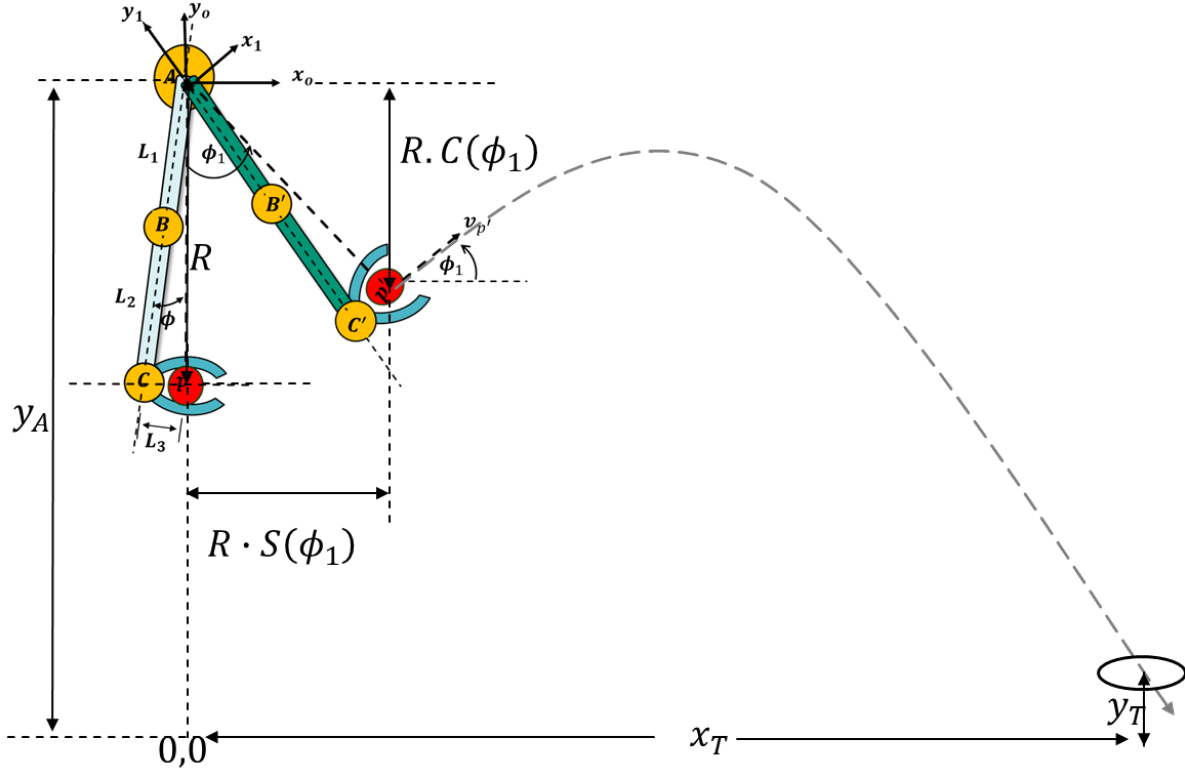


Figure 3.8: Description for bag flying diagram

Based on the figure 3.8, the distances that the projectile should cover in the  $x$  direction and the  $y$  direction are  $\Delta x = x_T - R \cdot S(\phi_1)$  and  $\Delta y = y_T - (y_A - R \cdot C(\phi_1))$  respectively. Thus, the optimum condition for the launching velocity and the angle is at :

$$\frac{d|\mathbf{v}_{p'}|^2}{d\phi_1} = 0 \quad (3.30)$$

And using equation 3.29 :

$$|\mathbf{v}_{p'}|^2 = \frac{G(\phi_1)}{K(\phi_1)} \quad (3.31)$$

where  $G(\phi_1) = g \cdot \Delta x$  and  $K(\phi_1) = S(2\phi_1) - 2 \cdot C^2(\phi_1) \cdot \frac{\Delta y}{\Delta x}$ .

Substituting equation 3.30 in equation 3.31 will lead to the following function :

$$\frac{d|\mathbf{v}_{p'}|^2}{d\phi_1} = \frac{K(\phi_1) \frac{dG(\phi_1)}{d\phi_1} - G(\phi_1) \frac{dK(\phi_1)}{d\phi_1}}{K(\phi_1)^2} = 0 \quad (3.32)$$

Working on the numerator given by :

$$f = K(\phi_1) \frac{dG(\phi_1)}{d\phi_1} - G(\phi_1) \frac{dK(\phi_1)}{d\phi_1} \quad (3.33)$$

And taking the derivative of this function  $f$  :

$$\frac{df}{d\phi_1} = K(\phi_1) \frac{d^2G(\phi_1)}{d\phi_1^2} - G(\phi_1) \frac{d^2K(\phi_1)}{d\phi_1^2} \quad (3.34)$$

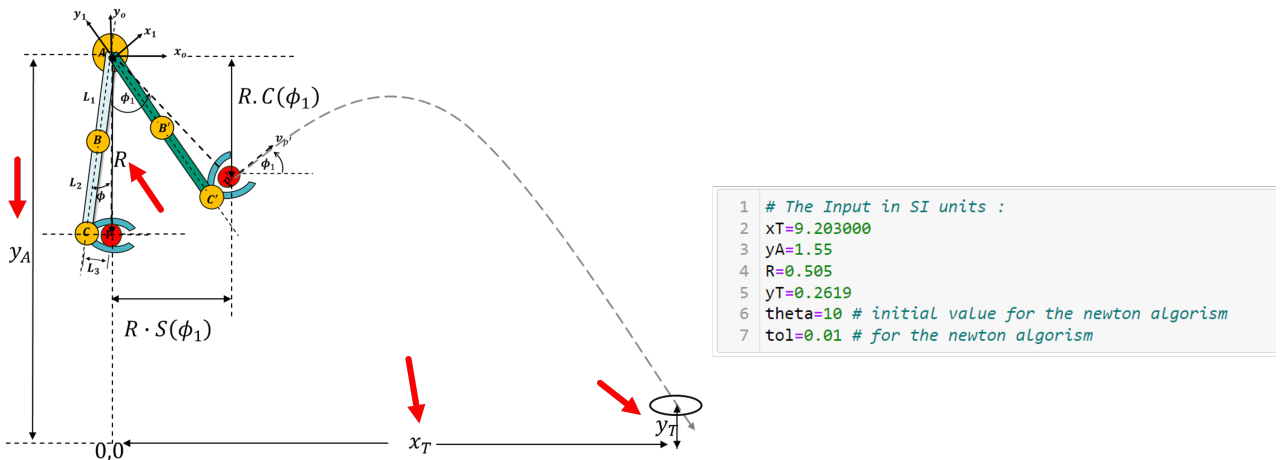


Figure 3.9: The input for python code to calculate the motion parameters

Using these derived formulas for Newton–Raphson method :

$$\phi_{1n+1} = \phi_{1n} - \frac{f}{f'} \quad (3.35)$$

This algorithm has been implemented in Python, where the inputs are as shown in figure 3.9. The output of this code is shown in two important figures, the first is figure 3.10 (a), which shows the values for the optimum launching velocity and angle. The second is figure 3.10 (b), which shows the final angular velocity that the arm should reach and the required time to reach such angular velocity. These are the values for the final angular velocity and the operation time that are shown earlier in figure 3.6.

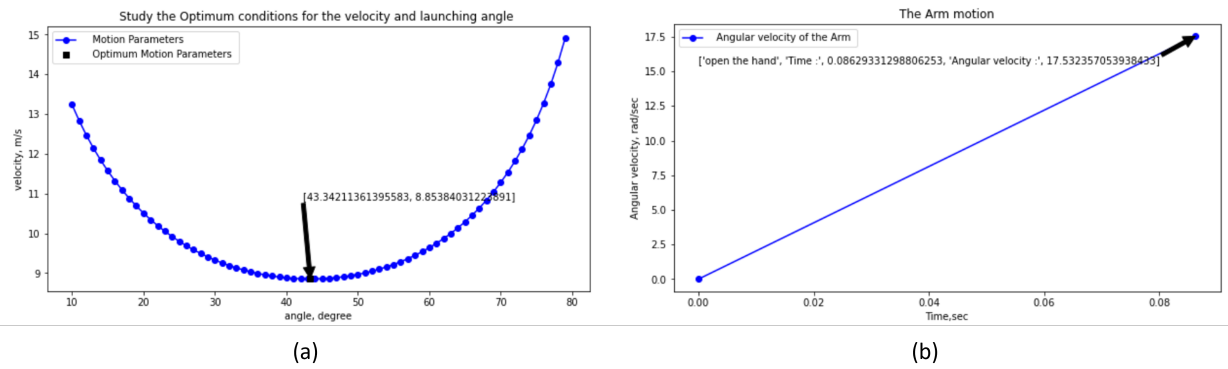


Figure 3.10: The motion parameters as output from the Python code

# Chapter 4

## Realistic Simulation for Corn-hole Game using Abaqus

In this chapter, an Abaqus model will be developed to simulate a realistic corn hole game based on the model proposed in section 3.1 and the optimization of this model as shown in section 3.3.

### 4.1 Abaqus Model Description

The description of this model is shown in figures 4.1 and 4.2. Four components have been created to simulate this game. All components are simulated as rigid bodies. The ball radius has been calculated so that it has the same volume as the corn bag, also the board dimensions are the standard dimensions (For the typical corn bag dimensions). The coefficient of friction between the corn-bag and the arm has been used as (0.1). The braking period (arm stopping period) has been used as 10 milliseconds . For the future work, a sliding experiment using the robot body material and the corn-bag fabric is important to identify the typical value for the coefficient of friction.

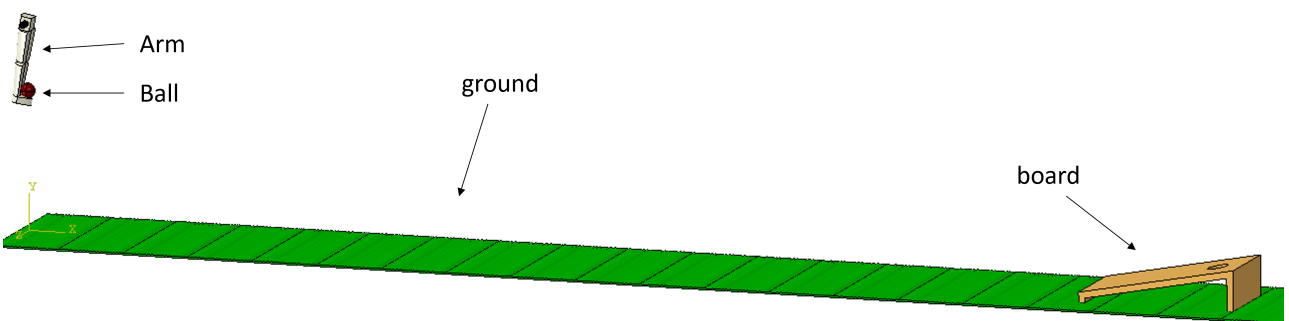


Figure 4.1: Realistic Simulation for Corn-hole Game using Abaqus

The boundary conditions applied on the arm are the motion parameters based on the inputs as shown in figure 4.3, where the simulation dimensions have been imported into the Python

code. Figure 4.4 illustrate the boundary conditions on the arm. So the arm is only allowed to rotate anticlockwise around the center of shoulder joint at the top of the arm, as shown in figure 4.4 (a). The rotation should reach the angular velocity, as calculated by the Python code in a give time period as shown in figure 4.4 (b) and (c). The braking period has been used as 10 milliseconds (The difference between 0.09629 and 0.08629 in figure 4.4 (b)). This period and the friction coefficient should be keep to the minimum possible values as to reduce the effect of friction-make it of insignificant effect. In case of a rough robot surface a layer of fabric with low coefficient of friction (0.1) attached to the robot hand could be very useful.

The boundary conditions on the ball are intended to simulate the mechanics of point mass motion, as shown in figure 4.5 . The rotation around the center of mass has been constrained as shown in figure 4.5 (a). The convention for units in Abaqus are tons for mass, Newton for force and mm for length. So the gravitational acceleration is  $9810 \text{ mm/s}^2$ , the mass of corn-bag is 0.0005 tons (=500 grams), thus the force is 4.905 N downwards, as shown in figure 4.5(b,c).

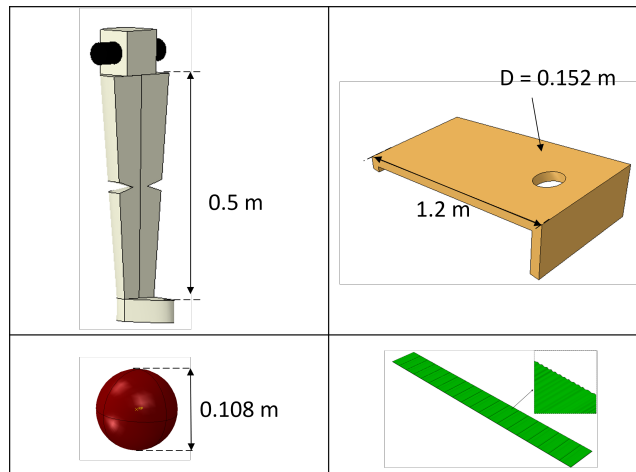


Figure 4.2: The dimensions of the components of the Corn-hole Game

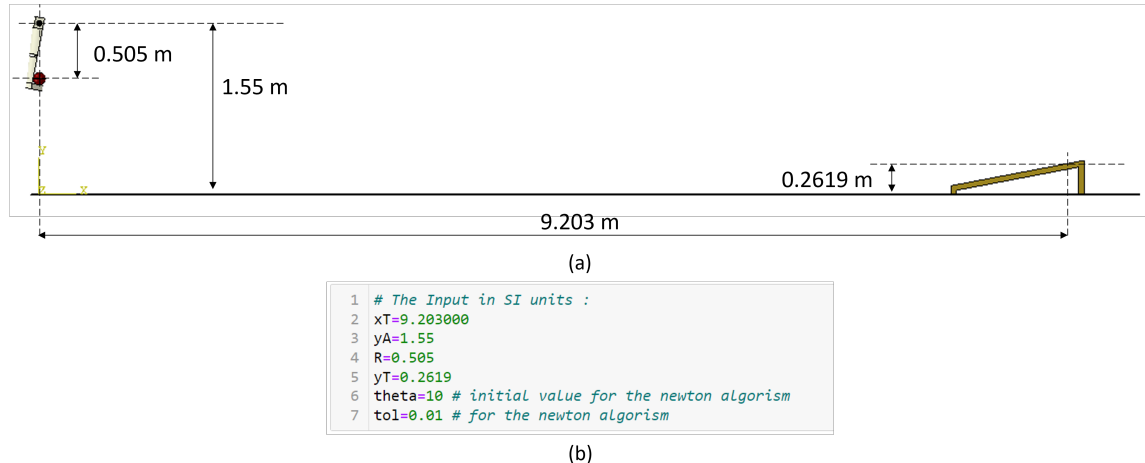


Figure 4.3: The input for python code to calculate the motion parameters

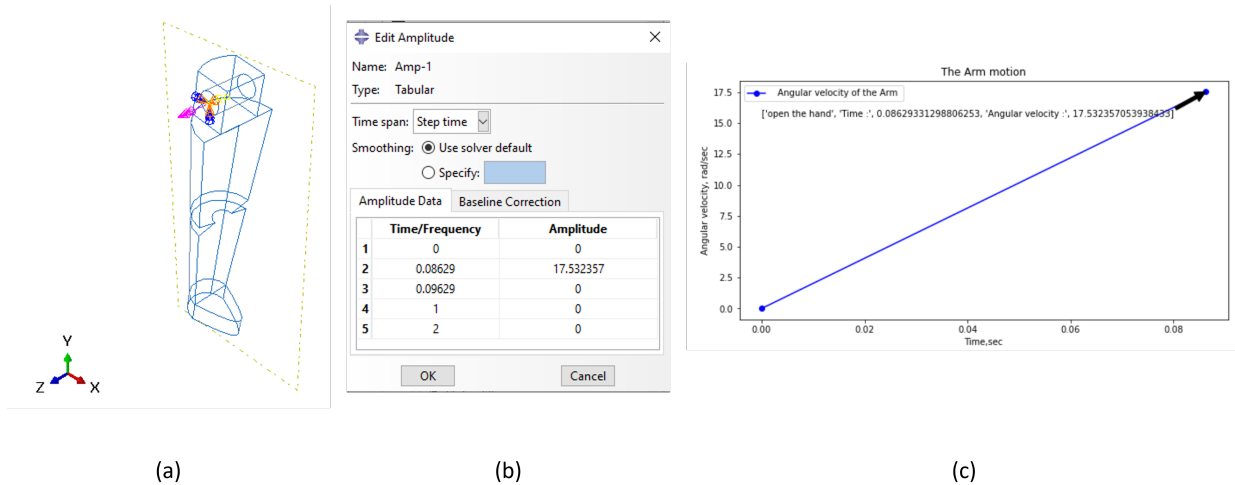


Figure 4.4: The boundary conditions applied on the arm

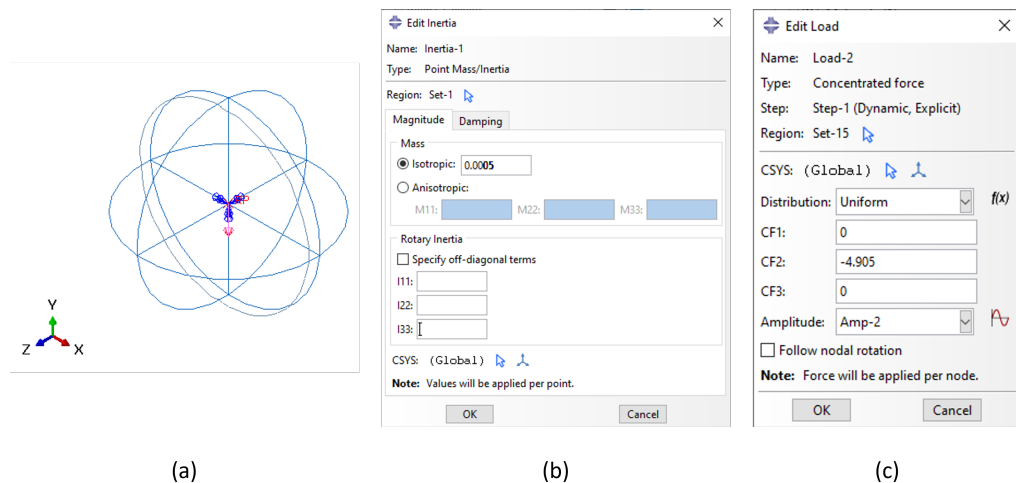


Figure 4.5: The boundary conditions applied on the ball

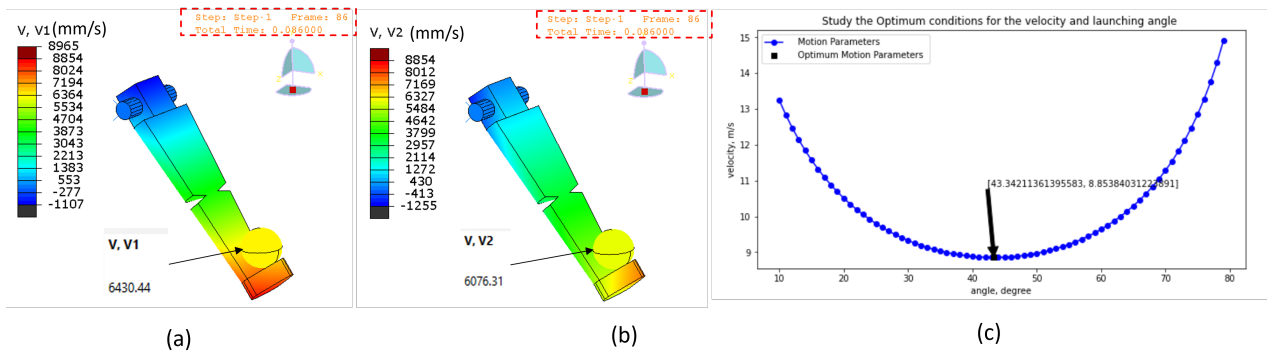


Figure 4.6: The analysis of the ball's velocity at launching point

## 4.2 Abaqus Model Results and Discussion

The analysis of the bag before launching is shown in figure 4.6(a,b), which is also showing the values for  $v_x$  and  $v_y$ . So, the velocity magnitude is 8.846 m/s , and the angle value at launching is  $\phi = \arctan\left(\frac{v_y}{v_x}\right) = 43.378^\circ$ , which are consistent with calculated values 4.6(c) . Also, figure 4.7(a)is showing the ball at almost half way, and (b) is at the point when the ball reaches the target.

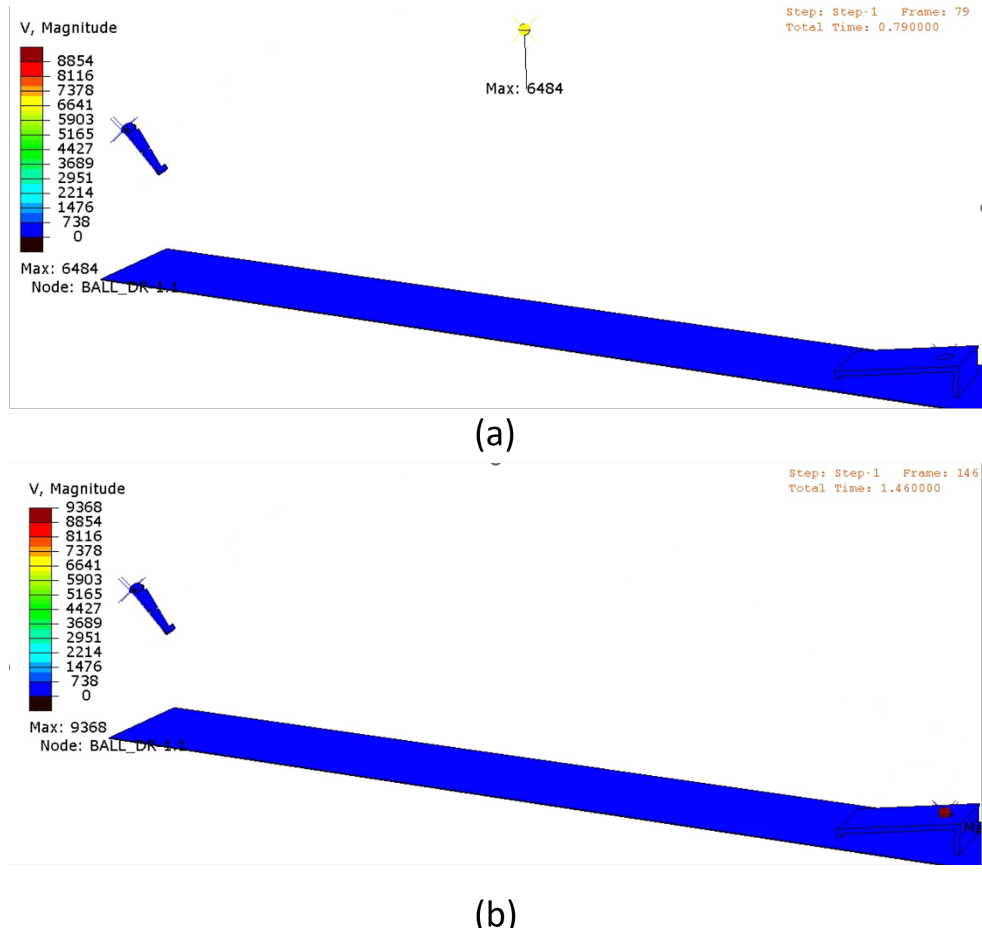


Figure 4.7: The motion of the ball during the simulation, the units of velocity is (mm/s). (a) is showing the ball at almost half way, and (b) shows the point when the ball reaches the target

# Chapter 5

## Conclusion and Future Work

In this work, it has been proven that the corn bag motion will follow the simple projectile motion model. A Python script to calculate the optimum motion parameters has been developed. Moreover, a realistic simulation for the cornhole game using Abaqus has been developed. For the future research, the work done in section 3.2 could be extended to account for simultaneous motion for the arm and the upper body using the same methods shown in section 3.1. In this context, the motion of the three joints constructing the arm could be studied and optimized. In this work, only the simple case has been studied, as it is very close to the realistic situation, however investigating other scenarios is recommended. Also, developing the simulation using robotics software could provide several advantages. In addition, the coefficient of friction is required, and a sliding experiment between the corn bag and hand could be helpful in determining this coefficient. Finally, studying the relation between the energy dissipation due to the friction and the braking period could be useful for more efficient and realistic calculations.

# Chapter 6

## References

1. Rato, D., Correia, F., Pereira, A. I., & Prada, R. (2022). Robots in games. *International Journal of Social Robotics*, 15(1), 37–57. <https://doi.org/10.1007/s12369-022-00944-4>.
2. Elite Special Events. (2019, December 17). Picnic Game Corn Hole | Elite Special Events. Elite Special Events | EliteSpecialEvents.Com. <https://elitespecialevents.com/product/picnic-game-corn-hole/>. Browsing date: 1st October 2023.
3. Serway, R., & Jewett, J. (2008). Physics for Scientists and Engineers with Modern Physics, Chapters 1-46. Thomson Brooks/Cole.
4. Torque and rotational motion tutorial. (n.d.). Physics. <https://www.physics.uoguelph.ca/torque-and-rotational-motion-tutorial>. Browsing date: 1st October 2023
5. Siciliano, B., Sciavicco, L., Villani, L., & Oriolo, G. (2010). *Robotics: Modelling, Planning and Control*. Springer Science & Business Media.